Experimental Evolution of Cell Shape in Bacteria

P.R.J. Yulo⌘[1], N. Desprat⌘[2,3], M.L. Gerth[4], Y. Liu[1], X.X. Zhang[1], P.B. Rainey[5,6,7] & H.L. Hendrickson[1,¥]

[1] *Institute of Natural and Mathematical Science, Massey University, Auckland.*
[2] *Laboratoire de Physique Statistique, Ecole Normale Supérieure, PSL Research University; Université Paris Diderot Sorbonne Paris-Cité; Sorbonne Universités UPMC Univeristés Paris 06; CNRS; 24 rue Lhomond, 75005 Paris, France.*
[3] *Paris Diderot University, 10 rue Alice Domon et Leonie Duquet. 75013 Paris, France.*
[4] *School of Biological Sciences, Victoria University of Wellington, PO Box 600, 6140, Wellington, New Zealand.*
[5] *New Zealand Institute for Advanced Study, Massey University, 0745, Auckland, New Zealand*
[6] *Department of Microbial Population Biology, Max Planck Institute for Evolutionary Biology, Plön, Germany.*
[7] *Laboratoire de Génétique de l'Evolution, Ecole Superieure de Physique et de Chimie Industrielles de la Ville de Paris (ESPCI Paris Tech), CNRS UMR 8231, PSL Research University, 75231 Paris, France.*

⌘These authors contributed equally to this work.

¥ Corresponding author, H.Hendrickson@massey.ac.nz

Cell shape is a fundamental property in bacterial kingdom. MreB is a protein that determines rod-like shape, and its deletion is generally lethal. Here, we deleted the *mreB* homolog from rod-shaped bacterium *Pseudomonas fluorescens* SBW25 and found that *ΔmreB* cells are viable, spherical cells with a 20% reduction in competitive fitness and high variability in cell size. We show that cell death, correlated with increased levels of elongation asymmetry between sister cells, accounts for the large fitness reduction. After a thousand generations in rich media, the fitness of evolved *ΔmreB* lines was restored to ancestral levels and cells regained symmetry and ancestral size, while maintaining spherical shape. Using population sequencing, we identified pbp1A, coding for a protein involved in cell wall synthesis, as the primary target for compensatory mutations of the *ΔmreB* genotype. Our findings suggest that reducing elongasome associated PBPs aids in the production of symmetric cells when MreB is absent.

Keywords: Cell shape, Evolution, Experimental Evolution, Coccoid, MreB, Pbp1A, OprD, Single cell analysis, Cell wall synthesis, Asymmetry.

1 Introduction

Bacterial cell shape is the result of the coordinated action of a suite of enzymes involved in cell wall construction, DNA segregation and cell division[1-6]. These are highly interdependent processes that can be difficult to genetically disentangle[7]. Cell shape is far from fixed on evolutionary time scales and is a key trait mediating bacterial fitness and adaptation[1]. Rod-like shape is hypothesized to be ancestral in bacteria but a myriad of shapes have successfully developed[5,8-10]. One of the key determinants of rod-like cell shape is MreB, the prokaryotic structural homolog of actin[11,12]. MreB is the molecular linchpin of rod-like shape and its loss is hypothesized to be either a primary or very early event in the transition between rod-like and spherical cell shape in bacteria[5,8-10,13-17].

MreB acts as a dynamic platform that directs the timing and location of a complex of cell wall elongation enzymes, the 'elongasome'[18] including the bi-functional lateral cell wall synthesis enzyme, Pencillin Binding Protein 1a (PBP1a)[19]. PBP1a and the other members of the elongasome complex move along the inner membrane of rod-like cells, manufacturing the growing peptidoglycan cell wall[20-23,24]. There is also growing evidence that MreB actively straightens cells during growth by associating with and directing the elongasome to regions of negative curvature in cell walls[25,26]. In addition, MreB disrupting studies, some using A22, demonstrate that the bundled MreB filaments participate in establishing the width and stiffness of the cell while exerting an inward force on the cell wall[26-30]. MreB is also known to have other pleitotropic effects on a range of cellular functions and its loss is frequently lethal in model microbial systems[12]. Some Δ*mreB* mutants can be grown for short periods in heavily supplemented media[15]. In A22 treated cells and in transiently viable *ΔmreB* strains the loss of *mreB* function leads to spherical shape and continuous volume increase, lysis and a loss of cell membrane potential [5,20,31-33].

Previous work has demonstrated the viability of *mreB*-defective transposon-generated mutants of otherwise rod-shaped *Pseudomonas fluorescens* SBW25[34]. These mutants produce spherical cells in standard Lysogeny Broth (LB) media. The discovery of a nascent spherical phenotype in the absence of MreB in a rod-like bacterium provides

71 the opportunity to investigate the consequences of MreB loss and the range of
72 compensatory mutations that might restore fitness.
73
74 Here we demonstrate that deletion of *mreB (ΔmreB)* in *P. fluorescens* SBW25 results
75 in viable spherical cells with decreased fitness and highly variable cell size. Evolving
76 this mutant for 1,000 generations in ten independent lineages led to recovery of both
77 WT fitness and cell volume whilst retaining spherical cell shape. Three primary
78 compensatory mutations are studied, two mutations in a PBP (Pencillin Binding
79 Protein) and a separate five-gene deletion. Morphological and single cell time-lapse
80 analysis of strains carrying these mutations demonstrate that these mutations affect
81 lateral cell wall synthesis and septation frequency, reducing sister cell growth
82 asymmetry and proliferation arrest in these cells. Finally, we use comparative
83 genomics of rod–like and spherical cells to infer that PBP loss is a common
84 phenomenon in the evolution of spherical species. Together, our results highlight
85 possible mutational routes by which rod-like cells can adapt their genetic machinery
86 to cope with MreB loss and spherical cell shape.
87
88
89 **2 Methods**
90
91 **Bacterial strains and culture conditions**
92 *Escherichia coli*, *Neisseria lactamica*, and *Staphylococcus aureus* were grown at
93 37°C, whilst *Lactococcus lactis* cremoris was grown at 30°C, and *P. fluorescens*
94 SBW25 at 28°C. Antibiotics were used at the following concentrations for *E. coli*
95 and/or *P. fluorescens* SBW25: 12 μg ml^{-1} tetracycline; 30 μg ml^{-1} kanamycin; 100 μg
96 ml^{-1} ampicillin. Bacteria were propagated in LB.
97
98 **Strain construction**
99 The *ΔmreB* strain was constructed using SOE-PCR (splicing by overlapping extension
100 using the polymerase chain reaction), followed by a two-step allelic exchange
101 protocol[1]. Genome sequencing confirmed the absence of suppressor mutations. The
102 same procedure was used to reconstruct the mutations from the evolved lines (PBP1a
103 G1450A, PBP1a A1084C, ΔPFLU4921-4925) into WT-SBW25 and the Δ*mreB*
104 backgrounds. DNA fragments flanking the gene of interest were amplified using two

105 primer pairs. The internal primers were designed to have overlapping complementary
106 sequences which allowed the resulting fragments to be joined together in a subsequent
107 PCR reaction. The resulting DNA product was TA-cloned into pCR8/GW/TOPO
108 (Invitrogen). This was then subcloned into the pUIC3 vector, which was mobilized
109 via conjugation into SBW25 using pRK2013. Transconjugants were selected on LB
110 plates supplemented with nitrofurantoin, tetracycline and X-gal. Allelic exchange
111 mutants identified as white colonies were obtained from cycloserine enrichment to
112 select against tetracycline resistant cells, and tetracycline sensitive clones were
113 examined for the deletion or mutations using PCR and DNA sequencing.
114
115 **Evolution Experiment**
116 Ten replicate populations of the Δ*mreB* strain were grown in 5 mL aliquots of LB
117 broth at 28°C with shaking at 180 rpm. Every 24 h, 5 μL was transferred to fresh
118 media. Every 5 days, samples of each population were collected and stored at -80°C
119 in 15% (v/v) glycerol. The number of generations per transfer changed over the
120 course of the experiment but is roughly ten generations per night and ~1,000
121 generations (100 transfers) were performed.
122
123 **Competitive fitness assay**
124 Competitive fitness was determined relative to SBW25 marked with GFP. This strain
125 was constructed using the mini-Tn7 transposon system, expressing GFP and a
126 gentamicin resistance marker in the chromosome (mini-Tn7(Gm)PrrnB P1 gfp-a)[2].
127
128 Strains were brought to exponential phase in shaken LB at 28°C before beginning the
129 competition. Competing strains were mixed with SBW25-GFP at a 1:1 ratio by
130 adding 150 uL of each strain to 5 mL LB, then grown under the same conditions for 3
131 hours. Initial ratios were determined by counting 100,000 cells using flow cytometry
132 (BD FACS Diva II). Suitable dilutions of the initial population were plated on LBA
133 plates to determine viable counts. The mixed culture was diluted 1,000-fold in LB,
134 then incubated at 28°C for 24 hours. Final viable counts and ratios were determined as
135 described above. The number of generations over 24 hours of growth were
136 determined using the formula ln(final population/initial population)/ln(2), as
137 previously described[3]. Selection coefficients were calculated using the regression
138 model s = [ln(R(t)/R(0))]/[t], where R is the ratio of the competing strain to SBW25-

139 GFP, and t is the number of generations. Control experiments were conducted to
140 determine the fitness cost of the GFP marker in SBW25. For each strain, the
141 competition assay was performed with a minimum of 3 replications. WT SBW25 had
142 a relative fitness of 1.0 when compared to the marked strain, indicating that the GFP
143 insert is neutral, and that the SBW25-GFP strain was a suitable reference strain for
144 this assay.
145
146 **Microscopy**
147 **Cells from liquid culture.** Cells were routinely grown in LB, and harvested at log
148 phase (OD_{600} 0.4). Viability assays were conducted using the LIVE/DEAD BacLight
149 Bacterial Viability Kit (Thermo Fisher). Viability was measured as the proportion of
150 live cells in the total population (live/(live +dead)). Nucleoid staining was done using
151 the DAPI nucleic acid stain (Thermo Fisher) following the manufacturer's protocols.
152
153 **Time-lapse on agarose pads.** Strains were inoculated in LB from glycerol stocks and
154 shaken overnight at 28°C. The next day, cultures were diluted 10^2 times in fresh LB
155 and seeded on a gel pad (1% agarose in LB). The preparation was sealed on a glass
156 coverslip with double-sided tape (Gene Frame, Fischer Scientific). A duct was cut
157 through the center of the pad to allow for oxygen diffusion into the gel. Temperature
158 was maintained at 30°C using a custom-made temperature controller[35].(Bacteria were
159 imaged on a custom built microscope using a 100X/NA 1.4 objective lens (Apo-ph3,
160 Olympus) and an Orca-Flash4.0 CMOS camera (Hamamatsu). Image acquisition and
161 microscope control were actuated with a LabView interface (National Instruments).
162 Typically, we monitored 10 different locations; images were taken every 5 min in
163 correlation mode[36]. Segmentation and cell lineage were computed using a MatLab
164 code implemented from Schnitzcell[37]. Bacteria were tracked for 3 generations.
165
166 **Scanning Electron Microscopy (SEM).** Cells were grown in LB, and harvested at
167 log phase. Cells were fixed in modified Karnovsky's fixative then placed between two
168 membrane filters (0.4μm, Isopore, Merck Millipore LTD) in an aluminum clamp.
169 Following three washes of phosphate buffer, the cells were dehydrated in a graded-
170 ethanol series, placed in liquid CO_2, then dried in a critical-point drying chamber. The
171 samples were mounted onto aluminum stubs and sputter coated with gold (BAL-TEC

172 SCD 005 sputter coater) and viewed in a FEI Quanta 200 scanning electron
173 microscope at an accelerating voltage of 20kV.
174
175 **Image analysis**
176 **Compactness and estimated volume measurements of cells from liquid culture.**
177 The main measure of cell shape, compactness or **C**, was computed by the CMEIAS
178 software as: (√4Area/π)/length. Estimated volume or $\mathbf{V_e}$ was estimated with different
179 formula, according to cell compactness, for spherical cells that have a compactness ≥
180 0.7, $\mathbf{V_e}$ was computed using the general formula for spheroids: $v=4/3\pi(L/2)(W/2)^2$,
181 where L=length and W=width. $\mathbf{V_e}$ of rod-shaped cells, defined as having a
182 compactness value ≤ 0.7, were computed using the combined formulas for cylinders
183 and spheres: $\mathbf{V_e} = (\pi(W/2)^2(L-W))+(4/3\pi(W/2)^3)$.
184
185 **Cell size, elongation rate, and division axis of cells on agarose pads.** Cell size was
186 computed as the area of the mask retrieved after image segmentation. The elongation
187 axis is given by the major axis of the ellipse that fits the mask of the cell. Division
188 axis is the computed by comparing the elongation axis between mother and sister cell,
189 through the following formula: $|\sin\theta|$, where θ is the angle between mother and
190 sister cell. We measured the elongation rate of individual bacteria by fitting the
191 temporal dynamics of cell area with a mono-exponential function. The elongation rate
192 is then given by the rate of the exponential. To obtain the intrinsic cell size and
193 disentangle it from the variability associated to asynchrony in the cell cycle, cell size
194 was measured at cell birth, i.e. right after septation. Cell size was then normalized to
195 the size of the WT strain.
196
197 **Proliferation probability.** For the first and second generations, we computed the
198 proliferation probability as the capability of progressing through the cell cycle and
199 dividing. Bacteria that do not grow or stop elongating before dividing are classified as
200 non-proliferating. For all non-proliferating bacteria, we confirmed that no division
201 occurs for the next 5 hours.
202
203 **Growth asymmetry.** For all sister cell pairs, we computed the asymmetry as the
204 contrast in cell elongation given by: $\left|\frac{r_2-r_1}{r_1+r_2}\right|$, where $r_{1,2}$ are the elongation rate of the

205 two sisters measured for the second generation. We then computed the population
206 average on the sub-population that proliferates in order to avoid trivial bias due to cell
207 proliferation arrest of one of the two sister cells.
208
209 **Protein sequence alignment and modeling**
210 Protein sequences were obtained from NCBI BLAST (http://blast.ncbi.nlm.nih.gov)
211 and The Pseudomonas Genome Database[38], and aligned using MEGA7[39]. The
212 sequence alignment was visualised using ESPript 'Easy Sequencing in PostScript' [40].
213
214 Protein visualisation was done on Visual Molecular Dynamics (VMD)[41] using the
215 crystal structure of *Acinetobacter baumannii* PBP1a in complex with Aztreonam as
216 the base model, which shares a 73% sequence identity (E value = 0.0) to the PBP1a of
217 *P. fluorescens* SBW25. Sequences were aligned, and locations of the mutations in the
218 evolved lines were mapped in the corresponding regions. The PDB file was
219 downloaded from the RCSB Protein Data Bank (www.rcsb.org) using PDB ID 3UE0.
220
221 **3 Results**
222 **MreB deletion in *P. fluorescens* SBW25 generates viable spherical cells**
223 Δ*mreB* cells to be spherical and display a highly variable cell size and shape
224 compared to the WT strain in phase contrast and SEM (Fig. 1A). The Δ*mreB* strain is
225 viable with approximately 82.5% (±7.9%) live cells compared to WT at 95.2%
226 (±1.2%)(Fig. 1B). Relative fitness in pairwise competition assays demonstrates that
227 the Δ*mreB* strain has a markedly lower relative fitness of 0.78 (±0.02) compared to
228 the WT (Fig. 1C)[42]. The Δ*mreB* strain had a slower generation time of 65 min (WT,
229 45 min), prolonged lag phase, and lower maximum yield (Supp. Fig. 1).
230
231 The *mreB* gene was ectopically expressed from the Tn7 site near the *glmS* region of
232 the Δ*mreB* strain completely restored WT morphology, viability, and relative fitness
233 in the *Δ mreB* cells with slightly delayed growth (longer lag) (Supp. Fig. 2).
234 Therefore the morphological effects seen in Δ*mreB* are considered to be due solely to
235 loss of MreB.
236

237 To quantify variability in size and shape we performed a principle components
238 analysis of the shape metrics (CMEIAS software package)[43,44] which motivated a
239 focus on a metric called compactness[4], a measure of the circularity of the cell's
240 outline. A compactness of 1.0 is circular whilst values below 0.7 are more typical of
241 rod-shaped cells. For our purposes, cells with an average compactness of 1.0 to 0.8,
242 before visible septation initiation are considered to be "spherical". The projected cell
243 outlines were used to estimate volume, (**V_e**) (see Material and Methods) and plotted
244 each cell's **V_e** vs compactness for both WT and *ΔmreB* cells (Fig. 1D).
245
246 WT cells have a small **V_e** range and a negative correlation between **V_e** and
247 compactness, reflecting the linear elongation and regular cell division of rod-shaped
248 cells. In contrast, the Δ*mreB* strain exhibits large spherical to ovoid cells (, with a
249 wide distribution of **V_e** ranging from 1.12 um^3 to ~90 um^3, averaging 20.65 um^3
250 (±16.17 um^3). Spherical *ΔmreB* cells initiate septation at a wide range of volumes
251 from 10 um^3 to 90 um^3, indicating that the relationship between cell size and division
252 is lost in *ΔmreB* cells (see lower compactness cells in Fig. 1D).
253
254 As cell volume increases, DNA content might also be expected to increase if DNA
255 replication continues irrespective of division frequency. Increased DNA content and
256 spherical cell shape are both predicted to further perturb cell division[45,46]. WT and
257 *ΔmreB* cells were stained with a nucleic acid stain (FITC) to label DNA and subjected
258 to flow cytometry. In both strains DNA content scaled with cell size as measured by
259 Forward Scatter Area (FSC-A). The largest *ΔmreB* cells have many times the DNA
260 content of WT cells, scaling roughly with volume (Fig. 1E, Supp. Fig. 3) indicating
261 that DNA replication continues irrespective of cell size. In addition, WT cells
262 observed by time-lapse, orientation of the division plane is consistent across divisions
263 ($|\sin(\phi)| = 0$). In contrast, in the *ΔmreB* population, septa positioned perpendicularly
264 relative to the last plane at each generation ($|(\sin(\phi)| = 1$) (Fig. 1F, Supp. Fig. 4B). The
265 change from maintaining septation angles to alternating septation suggests that DNA
266 segregation (prior to septation) is perturbed in cells that have lost rod-like shape. This
267 is consistent with similar results obtained from *E. coli* treated with the MreB inhibitor,
268 A22[47].
269
270 **Experimentally evolving spherical cells**

271 Having established that we have a viable *ΔmreB* in *P. fluorescens* SBW25 an
272 investigation into how this strain adapts to the challenge of MreB loss, was conducted
273 using an experimental evolution approach to select for mutants that restore fitness.
274 After 1,000 generations of evolution (Fig. 2A) the final evolved populations displayed
275 both relative fitness (Fig. 2B) and growth dynamics that were similar to the WT
276 (Supp. Fig. 5). However, the evolved cells remained spherical in shape (Fig. 2D,
277 Supp. Fig. 6). The size, however, as measured by **Ve** had decreased to roughly that of
278 the ancestral cells (Fig. 2D). The **Ve** of the evolved lines does not overlap with the
279 *ΔmreB* population (Fig. 1D), evidence that these evolved cells present a new
280 phenotype and are not a subset of the spherical *ΔmreB* ancestor. These newly evolved
281 spherical cells are most similar in cell shape, particularly at septation, to species like
282 *Lactococcus lactis* cremoris or *Neisseria lactamica* and other spherical bacterial
283 species that still undergo some elongation prior to division, not like *Staphylococcus*
284 *aureus* (Supp. Fig 11)[48]. The latter experience rapid division as nearly perfect spheres
285 (Supp. Fig.11) [49].
286
287 In order to understand the dynamics of the fitness recovery the frozen evolved
288 populations were resuscitated at various time points and competed these pairwise
289 against a GFP labeled WT ancestor (Fig. 2C). The fitness increase during evolution
290 occurred rapidly: after only 50 generations of growth, the evolved lines had an
291 average competitive fitness score of 0.92 (±0.01). This increased to an average fitness
292 of 0.97 (± 0.02) by the end of the experiment.
293
294 **Identifying mutations compensating for costs arising from deletion of *mreB* .**
295 The rapid fitness increase observed indicates that a small number of mutations arose
296 early and swept through the populations of poorly competing Δ*mreB* cells. In order to
297 identify these mutations, we conducted population sequencing at 500 and 1,000
298 generations and reference mapped these reads to the *P. fluorescens* SBW25 genome
299 (GCA_000009225.1) to an average read depth of 100 fold. We identified several
300 mutations affecting open reading frames that were found in over 75% of the sequence
301 reads in several evolved lines (detailed, Supp. Table 1). A single gene, *pbp1a* had
302 independent mutations in multiple lines. Representative *pbp1a* mutations from lines 1,
303 4 were chosen for further study. Line 7 had a five-gene deletion that included the
304 *oprD* homolog which was also chosen for further analysis.

305

306 The *pbp1A* gene (PFLU0406) encodes the major Class A penicillin-binding protein
307 responsible for the final steps of peptidoglycan synthesis. PBP1a proteins are key
308 components of peptidoglycan synthesis machinery in the cell wall elongation
309 complexes and are associated with the MreB cytoskeleton in rod-like cells[5].
310

311 This PBP1a contains three known domains (Fig. 3A). Structure mapping of the
312 mutations demonstrates that the mutation in Line 1 occurred in a well-conserved
313 region in the transpeptidase (TP) domain, proximal to the active site (Supp. Fig. 7).
314 Similar mutations in *Steptococcus pneumoniae*[50] cause a loss of function in this
315 domain. The mutation in Line 4 took place in the oligonucleotide/oligosaccharide
316 binding (OB) domain[6]. These will be referred to from hereon as the *pbp1a* Line 1 and
317 Line 4 mutations respectively. In order to determine the effects of these mutations on
318 cell shape and growth, these separately reconstructed in the WT and Δ*mreB*
319 backgrounds.
320

321 The *ΔmreB pbp1A* mutation strains remained spherical to ovoid, near WT volume and
322 DNA content (Fig. 3D, Supp. Fig. 9). These cells also retained the shorter generation
323 times (48 min), growth dynamics (Supp. Fig. 8) and relative fitness of the evolved
324 line populations (Fig. 3C), suggesting that the *pbp1A* mutations are each sufficient to
325 both restore WT fitness and to recapitulate the major phenotypes of evolved lines 1
326 and 4.
327 The function of PBP1A in the ancestral strain and therefore the presence of MreB, is
328 not well studied. The same mutations were therefore reconstructed in the WT
329 background. The WT *pbp1a* mutations also had generation times, growth curves
330 (Supp. Fig. 7) and relative fitness measures similar to WT (Fig. 3C).
331

332 The major phenotypic difference in the presence of the *pbp1a* mutations was that both
333 the *Pbp1a TP* and *OB* mutation reconstructions had rod-like cells that are significantly
334 narrower in cell widths (0.89 um ± 0.07, 0.94 um ± 0.05 respectively) compared to
335 WT (1.00 um ± 0.06) ($p = <0.001$). This resulted in smaller cell volumes (Fig. 3E and
336 Supp. Fig. 9). This decrease in cell width as a result of an amino acid change near the
337 transpeptidase domain of an elongasome-component is evidence that this mutation
338 decreases the function of PBP1a, likely by interfering with transpeptidase function

339 (Fig. 3E in Blue). The similar phenotype conferred by the OB domain indicates that
340 these domains act similarly in contributing to cell width (Fig. 3E in Green). The cell
341 size decrease also corresponded with a slight decrease in DNA content (Supp. Fig. 3).
342 The production of thinner cells, is consistent with previous work on the effects of
343 PBP1a function loss in both *B. subtilis* and in *E. coli* [51-54]. Based on the positions of
344 the respective mutations, and their resulting phenotypes in WT cells, we interpret
345 these results to indicate that either of these *pbp1A* mutations can reduce lateral cell
346 wall synthesis, resulting in smaller cells when MreB is present.
347
348 The other major mutation identified in the evolved lines was a five-gene deletion
349 (PFLU4921-4925) in evolved Line 7 (Fig. 3B, Supp. Table 1). The deletion contains
350 three hypothetical proteins, a cold shock protein (PFLU4922, encoding CspC), and an
351 outer membrane porin, PFLU4925 which encodes OprD. The latter is responsible for
352 the influx of basic amino acids and some antibiotics into the bacterial cell[7]. This
353 deletion was constructed and characterised in the Δ*mreB* and WT backgrounds.
354
355 The Δ*mreB* five-gene deletion strain had a generation time and growth dynamics
356 similar to WT, with an additional extended lag time (Supp. Fig. 8). The viability and
357 relative fitness were also highly similar to WT (Fig. 3C). The cells were spherical
358 with an averge **Ve** of 5.32 um^3 (±3.18) (Fig. 3D and Supp. Fig. 8). As in the *pbp1A*
359 Line 1 and Line 4 mutations, DNA content was also decreased compared to the
360 *ΔmreB* ancestor (Supp. Fig. 3). In addition, the five-gene deletion produces cell
361 division defects in 25.61% (±6.42%) of these cells, manifesting as septation defects
362 and connected clumps of spherical cells (Fig 3D, Supp. Fig. 9).
363
364 In the WT strain, the five-gene deletion produced rod shaped cells with growth
365 characteristics similar to the WT strain (Supp. Fig 8). These cells were however
366 significantly thinner than WT (width = 0.74um ± 0.06, p = <0.001) and had a smaller
367 average **Ve** of 2.47 um^3 (±1.18) (Fig. 3E and Supp. Fig. 8). As in the *ΔmreB*
368 background, a sub-population exhibits a filamenting phenotype occurring in 20% (±
369 4%) of the population. The five-gene deletion strains were the only ones that showed
370 evidence of dispersed DNA between incomplete septa in DAPI staining (Supp. Fig
371 S10). Intriguingly, clinically isolated *Pseudomonas* with *oprD* deletions have
372 significant changes in the regulation of the MinCD system[55]. In closely related model

373 systems MinCD, acts to negatively affect septal placement by poles and accumulating
374 as a result of cell shape asymmetry[17,56-58]. The connection between OprD and MinCD
375 in *Pseudomonas* merits further investigation but *oprD* loss may mitigate large cell
376 size and increase fitness in *ΔmreB* by retuning septation frequencies. This would also
377 imply that the viable *ΔmreB* cells lack proper the geometry required to support
378 MinCD oscillations[59], resulting in erratic septation and driving large cell size.
379
380 **Sister Cell Asymmetry at the Single Cell Level**
381 In order to determine the basis of the fitness cost of the mreB deletion, we, we
382 conducted single cell experiments in the reconstructed mutants and representative
383 evolved clones from lines 1, 4 & 7. Time-lapse microscopy was used to track
384 individual cells through subsequent generations to measure size, elongation rate,
385 division axis and shape for each cell as well as their capacity to produce two
386 daughters[36,60].
387
388 All reconstructed strains except the strain that ectopically expresses *mreB* (closed
389 grey square), have a reduced rate of cell wall synthesis relative to the WT (Fig. 4A)
390 but all are higher than the ancestral *ΔmreB* strain. Cell elongation rates are higher in
391 the presence of MreB in the *pbp1A* Line 4 mutant, but not the Line 1 mutant,
392 suggesting that the transpeptidase domain mutation may affect the degree to which
393 MreB stimulates synthesis[61].
394
395 In addition, single cell experiments measured that a fraction of cells underwent
396 persistent proliferation arrest on solid media, even after five hours of observation (Fig.
397 4B). Tracking pairs of dividing cells coming from the same mother revealed that they
398 experience unequal rates of cell wall synthesis, or 'growth asymmetry' (Fig. 4B). A
399 strong correlation is observed between proliferation arrest and growth asymmetry in
400 our reconstructed mutation strains and representative clones. In strains that had higher
401 growth asymmetry, more proliferation arrest was observed (Fig 4D). This increased
402 growth asymmetry might either initiate proliferation arrest or both features may be
403 symptoms of another attribute of these cells such as cell size or defects in DNA
404 segregation driven by cell shape and septum aberrations[46,62].
405

406 Accordingly, cells that have lost MreB are able to find a new equilibrium by
407 decreasing elongation synthesis (*pbp1A* mutations) or possibly modulating septation
408 associated synthesis (the *oprD* inclusive deletion). Either serves to increase the
409 relative proportion of synthesis at the septum, and decrease elongasome associated
410 synthesis. The advantage gained through these adjustments in response to MreB loss
411 hint at a previously unrecognized role of MreB in ensuring the equal partitioning of
412 the elongasome components before and after cell division.
413
414 **Recapitulating spherical shape evolution**
415 These experiments demonstrate that either a decrease in activity in a PBP in the
416 elongasome or a five-gene deletion that includes *oprD* allow a rebound in fitness
417 when *mreB* is lost. It was previously reported that coccoid bacterial species have
418 lower estimated numbers of PBPs based on estimates from a biochemical function
419 assay[63]. We were therefore interested in whether comparative genomics of completely
420 sequenced bacteria bore this pattern out as well. We therefore selected 26 bacterial
421 species pairs in which one member has maintained rod-like shape and the other has
422 become spherical and compared the abundance of the homologues of the genes
423 implicated in our evolution experiment; MreB, PBPs and OprD homologs. OprD
424 homologs were too rare across species to analyze. However, we observed a significant
425 relationship between coccoid lineages that had lost MreB and a decrease in the
426 number of PBP homologs (avg. PBPs in rods = 9.22 ± 5.15; spheres = 3.89 ± 2.65;
427 difference: $p = <0.001$). From this we infer that species that have naturally evolved
428 from rod-like to spherical shape tend to have lost both *mreB* and approximately half
429 of their PBP genes.
430
431 **Reshaping a rod-like pseudomonad to be a spherical cell**
432 *P. fluorescens* SBW25 is a rod-like bacterium that can be reshaped into a rapidly
433 growing spherical cell in as little as two mutational steps, the deletion of *mreB* and
434 either a single amino acid changing mutation in *pbp1A* or an *oprD* inclusive deletion.
435 The reason that this strain is tolerant of MreB loss is not currently known but a
436 separate paralog does not exist in this strain.
437
438 The loss of MreB from the ancestral SBW25 causes extremely large cells with
439 multiple chromosomes (Fig. 1D,E) with highly irregular septation. In addition, sister

440 cells elongate perpendicularly to mother cells, across cell divisions (Fig 1E-F),
441 consistent with MreB disruption experiments using i*li* and *P. aeriginosa*[31,64]. Both cell
442 wall synthesis and DNA replication are continuous in these cells (Fig. 1E and Fig.
443 4A) meaning that large cell size is the result of a reduction in septation frequency,
444 maybe due to the loss of the ordered relationship between septation and DNA
445 segregation in spherical cells[46].
446
447 The *ΔmreB* population had high levels of cell wall synthesis asymmetry and while
448 either of the *pbp1A* mutations increased this symmetry, the five-gene deletion did not
449 (Fig. 4D). This increase in symmetry suggests that the distribution of active
450 elongasomes may be disorganised in cells lacking MreB and that this disorganization
451 is reduced when *pbp1A* is mutated[52](Fig 4C). This raises the possibility that symmetry
452 in cell synthesis is maintained in these cells by continued septal cell wall synthesis.
453 While this is consistent with models of other spherically shaped cells in which much
454 of the cell wall synthesis further investigation of cell wall synthesis is required to
455 support or refute this hypothesis[65-67].
456
457 **Implications for the evolution of spherical cell shape**
458 The wide array of cell shapes and sizes observed in the eubacteria have arisen from an
459 ancestral rod-like cell shape[2,68-70] Coccoid or spherical cells are the product of a
460 degradation of this shape[14,71]. The transition to spherical cell shape has taken place
461 independently many times[8,72-74] and is associated with *mreB* loss, possibly as an early
462 event[48,49].
463
464 This study uncovers separate compensatory mutations that allow rapid fitness
465 recovery after MreB loss. If MreB loss is a common early event in coccus evolution
466 then there are likely to be both genetic and environmental contexts that favor this
467 state[2,9,14,71]. One possibility is that the transient increase in cell size observed in
468 Δ*mreB* cells is advantageous in some settings. This hypothesis compels further
469 investigation[16].
470
471
472 **4 Conclusions**
473 Cell shape is a fundamental property of cells that defines motility, DNA segregation,

474 replication, nutrient acquisition, waste elimination and predator evasion[16]. *P.*
475 *fluorescens* SBW25 is a rod-shaped bacterium that is amenable to MreB deletion.
476 The loss of MreB is a non-lethal but deleterious event that leads to irregular, large-
477 sized spherical cells. Further, separate mutations can restore fitness and volume whilst
478 retaining spherical cell shape and these are likely decrease-of-function mutations in
479 the gene encoding elongasome member PBP1A, or a five-gene deletion that includes
480 *oprD*. These mutations are able to restore symmetry in cell growth between sister
481 cells and decrease cell death. We therefore propose a model of molecular change
482 when MreB is lost, essentially re-storing symmetric cell wall synthesis by relying
483 more heavily on synthesis at the septum. Last, our study implicates a decrease of PBP
484 function, as a general strategy in cells recovering from the loss of MreB and refining
485 spherical cell shape in bacteria.
486
487 **Acknowledgements**
488
489 We thank Olin Silander for helpful discussions and for his assistance to PRY with
490 principle components analysis of cell shape, Sebastian Schmeier and Saumya
491 Agrawal for bioinformatic analysis and Tim Cooper for helpful comments on the
492 manuscript. Electron Microscopy was provided by Massey University and was
493 performed by Niki Murray, Manawatu Microscopy and Imaging Centre, Massey
494 University, Palmerston North, NZ.
495
496 **Figures**
497

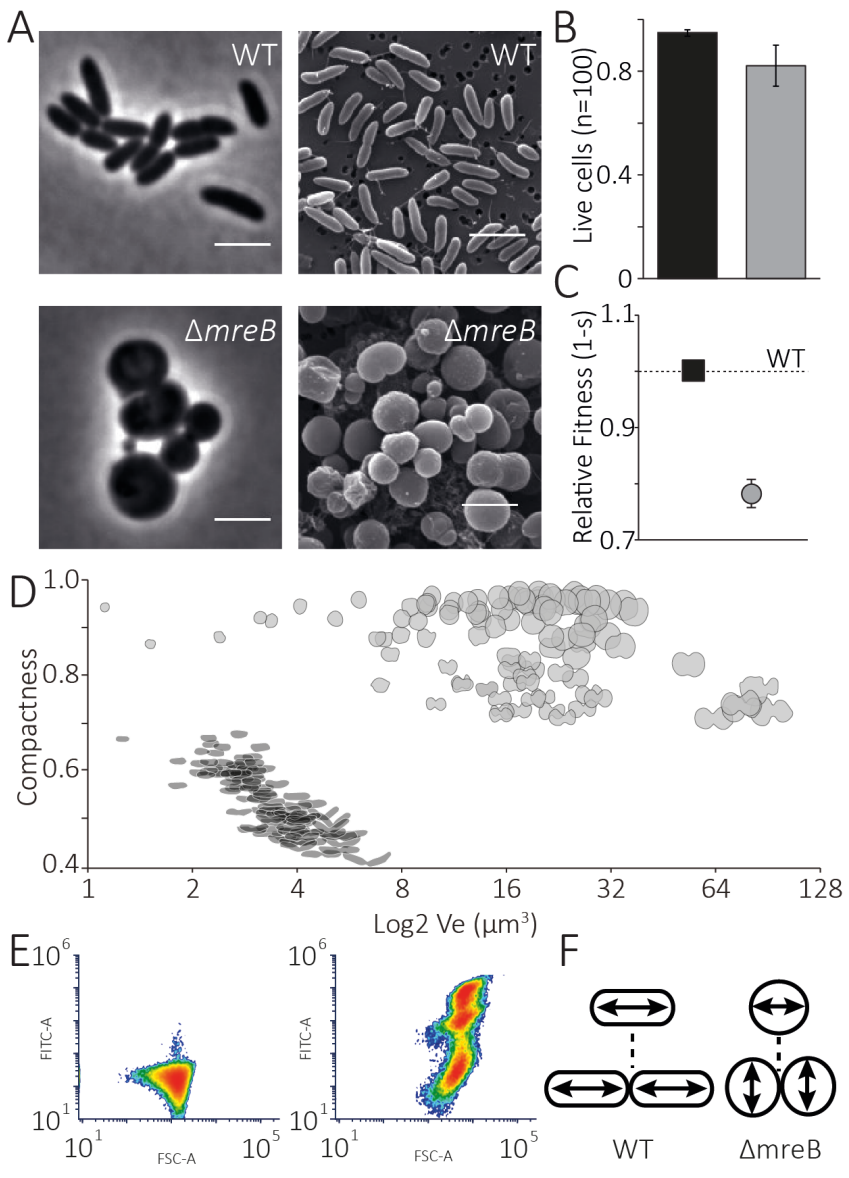

Figure 1. Characterisation of WT and Δ*mreB* strains. Figure shows (A) photomicrographs of WT and Δ*mreB*. Scale bars, 3 µm. B) Proportion of live cells in WT (black bar) and Δ*mreB* (grey bar). Error bars represent standard error (n = 3). C) Fitness of WT GFP and the ancestral Δ*mreB* mutant relative to WT when both are in exponential phase during pairwise competition assays. Error bars as in 1B. D) The relationship between cell shape and estimated volume (V_e) is represented using compactness, a measure of roundness. One hundred representative cells from each WT and Δ*mreB* are shown as cell outlines. E) DNA content (FITC-A) is highly correlated with increased cell sizes (FSC-A) in Δ*mreB* but both are limited in WT cells (n=50,000 events). F) Diagram of WT cells maintaining a single consistent division plane whilst Δ*mreB* cells alternate division planes by 90° from one division to the next.

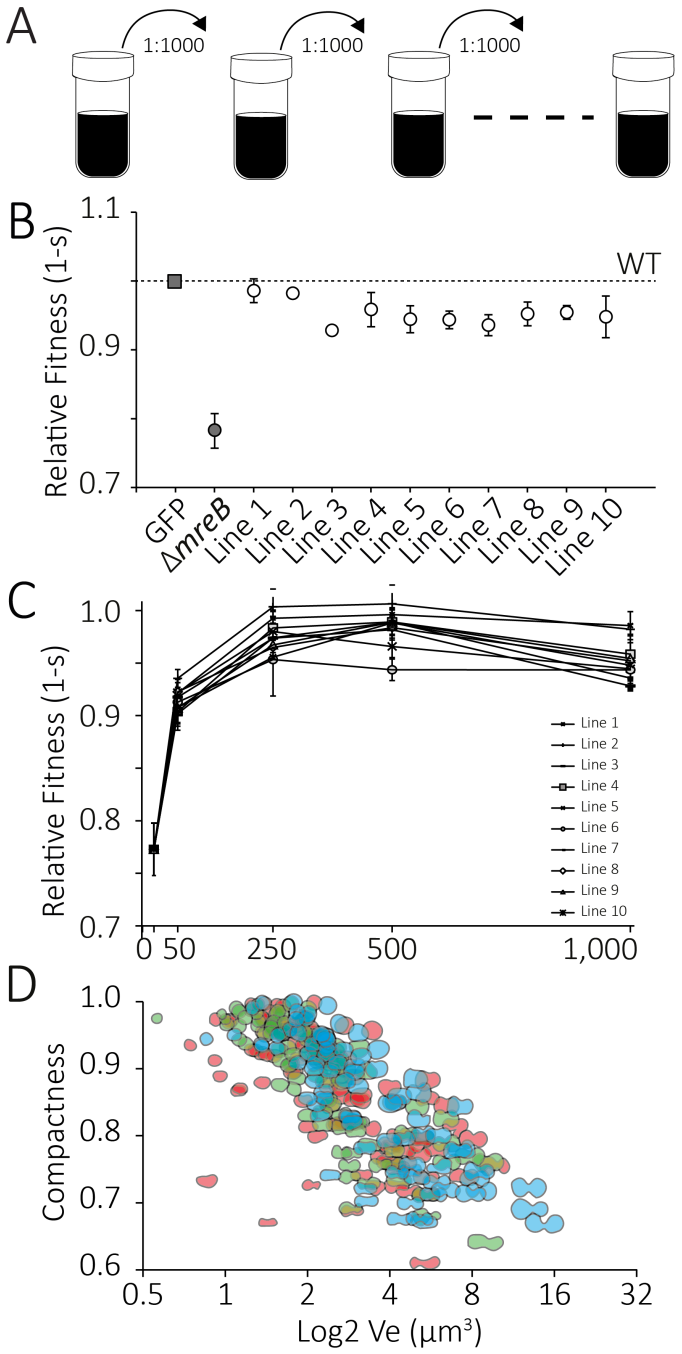

Figure 2. Characterisation of Evolved Lines at 1,000 generations. A) Diagram of evolution experiment protocol. 1:1000 transfer each 24 hours. B) Relative fitness of the Δ*mreB* mutant and evolved lines after ~1,000 generations relative to WT (dashed line) in pairwise competition experiments. Error bars represent standard error (n = 3). C) Relative fitness of the evolved lines during 1,000 generations of growth. Error bars as in B. D) Cell outlines of three representative evolved lines Line 1 in blue, Line 4 in green and line 7 in red. One-hundred randomly chosen cell outlines from each line are depicted.

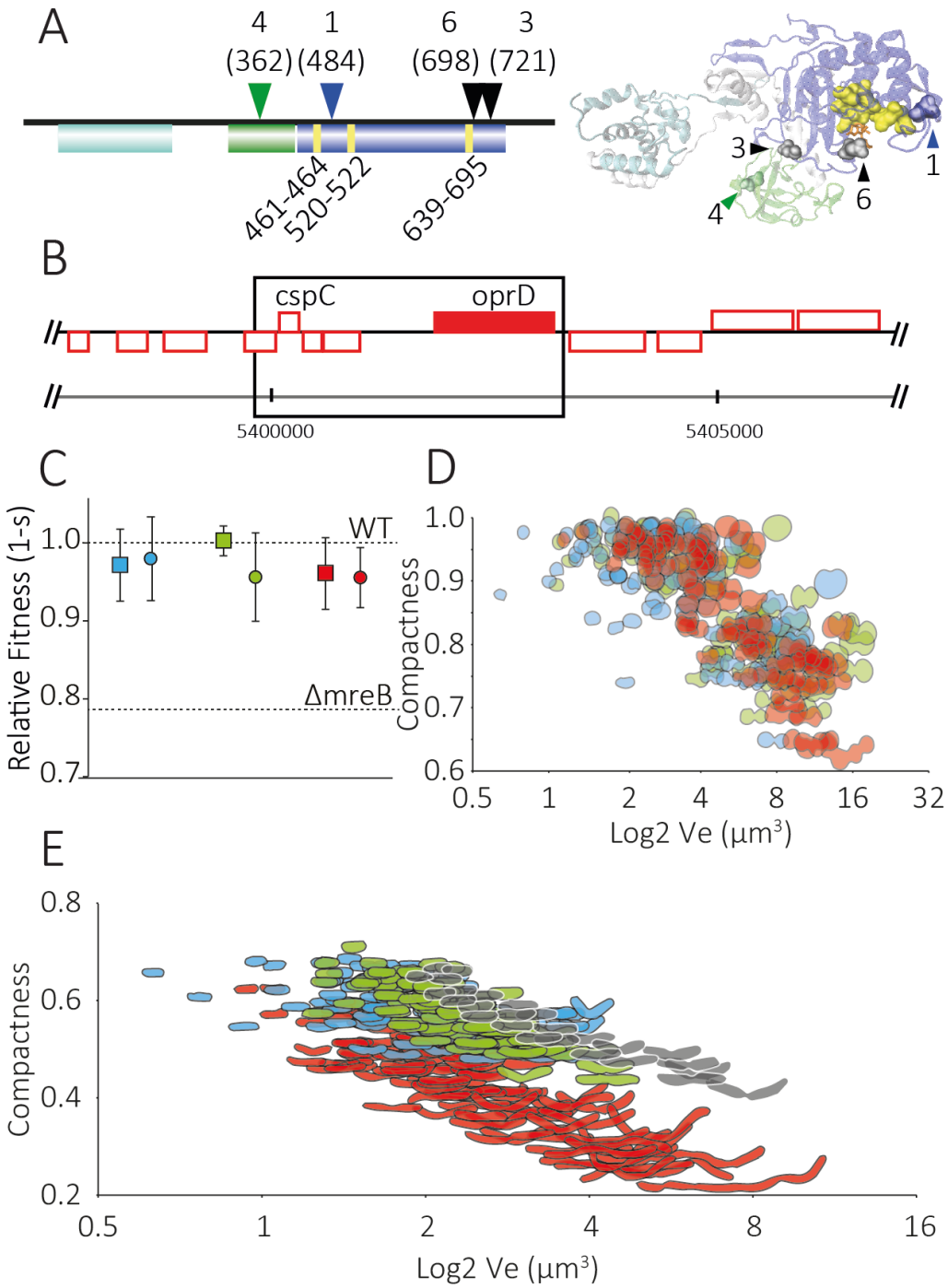

Figure 3. Characterisation of the reconstructed mutations in WT and Δ*mreB* background. A) Domain map and model of PBP1a (PFLU0406) showing the 2 major active sites; the glycosyltransferase (GT) domain (cyan) and the transpeptidase (TP) domain (blue). The oligonucleotide/oligosaccharide binding (OB) domain is shown in green. The active site of the TP domain is also shown (yellow). The mutations identified are indicated above the map. B) Genome map of *oprD* inclusive deletion, (PFLU4921-PFLU4925) and surrounding region. Genes with function calls are noted. C) Relative fitness of the three reconstructed mutants in the Δ*mreB* (circles) and WT

575 (squares) backgrounds. Line 1 reconstruction, PBP1a D484N is shown in blue, Line 4
576 PBP1a T362P is shown in green and the OprD containing deletion reconstruction is
577 shown in red. D) Compactness versus estimated volume (Ve) for reconstruction
578 strains in the Δ*mreB* background, colors as in 1C (N=100). E) Compactness versus
579 estimated volume (Ve) of the mutants in the WT background colours and N as in C
580 and D. A subset of WT cells are shown in light grey for comparison.
581
582

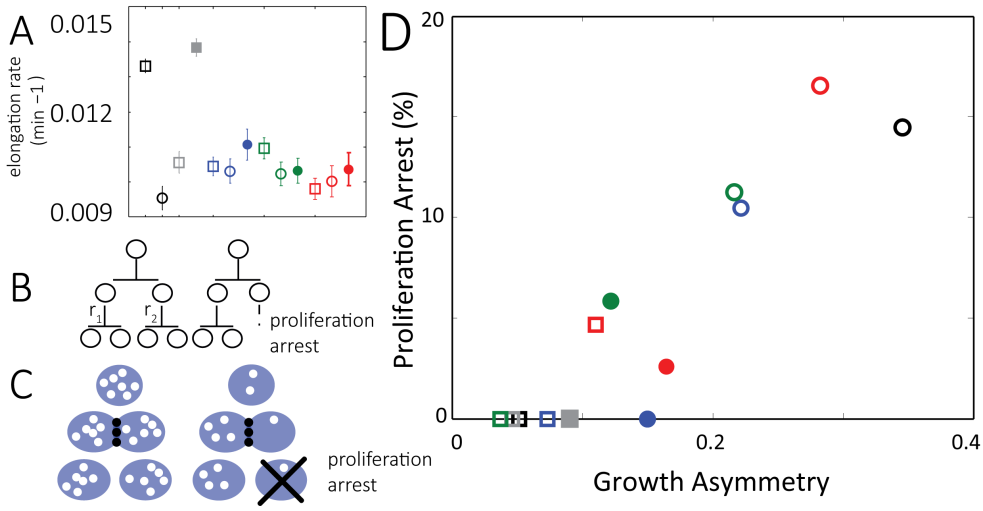

583

584

585 Figure 4. Single cell time-lapse measurements of reconstructed mutations. A) Average
586 population elongation rate for WT, reconstructions and evolved cells. Open square
587 data points represent WT or WT and respective mutations (open grey square = *ΔmreB*
588 with ectopic *mreB*), open circles are Δ*mreB* or *ΔmreB* and respective mutations and
589 closed symbols are evolved cell lines. Colors as in Fig 3; blue is Line 1 or PBP1a
590 D484N, green is Line 4 or PBP1a T362P, red is Line 7 or OprD inclusive deletion. B)
591 Strategy for analyzing single cell measurements during growth on agarose pads
592 including r_1 and r_2. C) Model for relationship between growth asymmetry and
593 proliferation arrest driven by disordered acquisition of cell wall synthesis machinery
594 (white dots). The septum associated PBPs (black circles) at the division plane provide
595 symmetric cell wall synthesis to respective daughter cells. D) Relationship between
596 paired-sister cell proliferation arrest and growth asymmetry in all reconstructions and
597 representative evolved cells (N=100 for each).

598

599

600

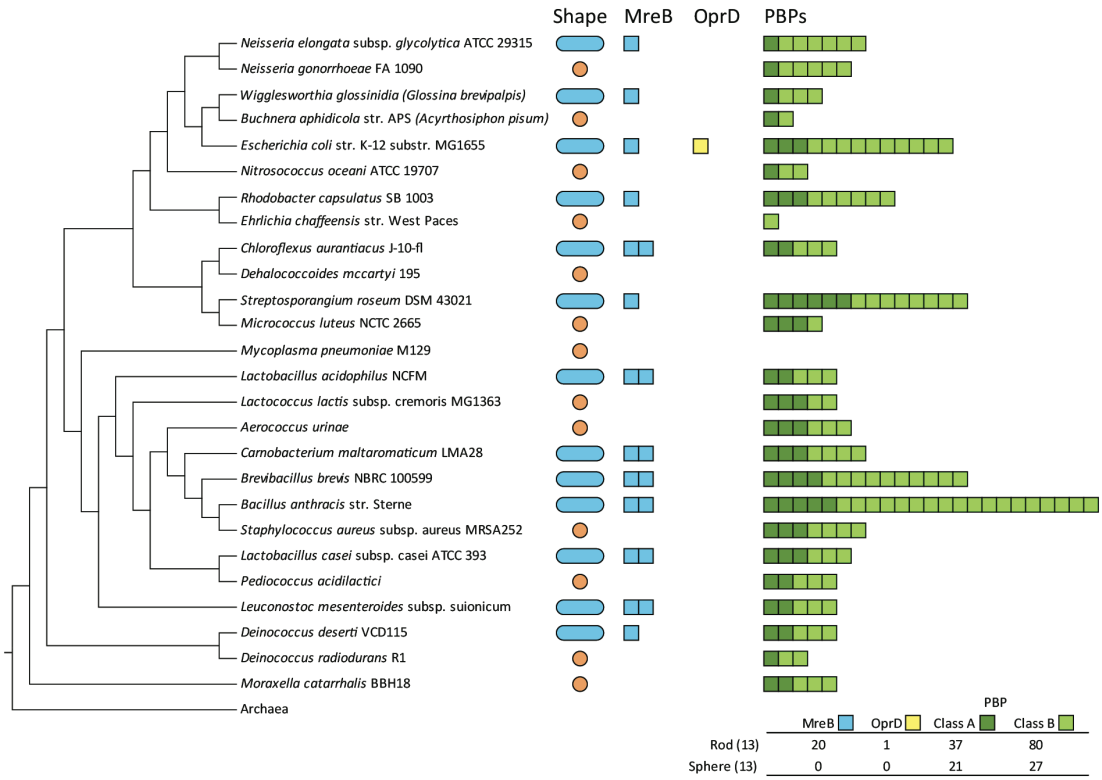

Figure 5. Penicillin-Binding Proteins (PBPs) is observed in extant spherically-shaped cells. A selection of 26 paired rod-shaped and spherical cells were analyzed for their PBP and OprD homologs. The genomes of naturally evolved spherical cells have fewer PBPs than rod-shaped species. OprD homologs were rare.

References:

1. Young, K. D. Bacterial morphology: why have different shapes? *Curr Opin Microbiol* **10,** 596–600 (2007).
2. Young, K. D. Bacterial shape. *Mol Microbiol* **49,** 571–580 (2003).
3. Young, K. D. Bacterial shape: two-dimensional questions and possibilities. *Annu. Rev. Microbiol.* **64,** 223–240 (2010).
4. Huang, K. C., Mukhopadhyay, R., Wen, B., Gitai, Z. & Wingreen, N. S. Cell shape and cell-wall organization in Gram-negative bacteria. *Proc Natl Acad Sci USA* **105,** 19282–19287 (2008).
5. Daniel, R. A. & Errington, J. Control of cell morphogenesis in bacteria: two distinct ways to make a rod-shaped cell. *Cell* **113,** 767–776 (2003).
6. Osborn, M. J. & Rothfield, L. Cell shape determination in Escherichia coli. *Curr Opin Microbiol* **10,** 606–610 (2007).
7. van Teeffelen, S. *et al.* The bacterial actin MreB rotates, and rotation depends on cell-wall assembly. *Proc Natl Acad Sci USA* **108,** 15822–15827 (2011).
8. Siefert, J. L. & Fox, G. E. Phylogenetic mapping of bacterial morphology. *Microbiology (Reading, Engl.)* **144 (Pt 10),** 2803–2808 (1998).
9. Veyrier, F. J. *et al.* Common Cell Shape Evolution of Two Nasopharyngeal Pathogens. *PLoS Genet.* **11,** e1005338 (2015).
10. Margolin, W. Sculpting the bacterial cell. *Curr Biol* **19,** R812–22 (2009).
11. Strahl, H., Bürmann, F. & Hamoen, L. W. The actin homologue MreB organizes the bacterial cell membrane. *Nat Commun* **5,** 3442 (2014).
12. Shaevitz, J. W. & Gitai, Z. The Structure and Function of Bacterial Actin Homologs. *Cold Spring Harbor Perspectives in Biology* **2,** a000364–a000364 (2010).
13. Tamames, J., González-Moreno, M. & Mingorance, J. Bringing gene order into bacterial shape. *TRENDS in …* (2001).
14. Baidouri, El, F., Venditti, C. & Humphries, S. Independent evolution of shape and motility allows evolutionary flexibility in Firmicutes bacteria. *Nat. ecol. evol.* **1,** 0009–6 (2016).
15. Formstone, A. & Errington, J. A magnesium-dependent mreB null mutant: implications for the role of mreB in Bacillus subtilis. **55,** 1646–1657 (2005).
16. Young, K. D. The selective value of bacterial shape. *Microbiol Mol Biol Rev* **70,** 660–703 (2006).
17. Pichoff, S. & Lutkenhaus, J. Overview of cell shape: cytoskeletons shape bacterial cells. *Curr Opin Microbiol* **10,** 601–605 (2007).
18. Szwedziak, P. & Löwe, J. Do the divisome and elongasome share a common evolutionary past? *Curr Opin Microbiol* **16,** 745–751 (2013).
19. Zhao, H., Patel, V., Helmann, J. D. & Dörr, T. Don't let sleeping dogmas lie: New views of peptidoglycan synthesis and its regulation. *Mol Microbiol* (2017). doi:10.1111/mmi.13853
20. Figge, R. M., Divakaruni, A. V. & Gober, J. W. MreB, the cell shape-determining bacterial actin homologue, co-ordinates cell wall morphogenesis in Caulobacter crescentus. *Mol Microbiol* (2004).
21. Ouzounov, N. *et al.* MreB Orientation Correlates with Cell Diameter in Escherichia coli. *Biophysj* **111,** 1035–1043 (2016).
22. Garner, E. C. *et al.* Coupled, circumferential motions of the cell wall synthesis machinery and MreB filaments in B. subtilis. *Science* **333,** 222–225 (2011).
23. Cava, F., Kuru, E., Brun, Y. V. & de Pedro, M. A. Modes of cell wall growth

differentiation in rod-shaped bacteria. *Curr Opin Microbiol* **16,** 731–737 (2013).
24. Domínguez-Escobar, J. *et al.* Processive movement of MreB-associated cell wall biosynthetic complexes in bacteria. *Science* **333,** 225–228 (2011).
25. Tropini, C. *et al.* Principles of Bacterial Cell-Size Determination Revealed by Cell-Wall Synthesis Perturbations. *CellReports* **9,** 1520–1527 (2014).
26. Ursell, T. S. *et al.* Rod-like bacterial shape is maintained by feedback between cell curvature and cytoskeletal localization. *Proc Natl Acad Sci USA* **111,** E1025–34 (2014).
27. Sun, S. X. & Jiang, H. Physics of bacterial morphogenesis. *Microbiol Mol Biol Rev* **75,** 543–565 (2011).
28. Tuson, H. H. *et al.* Measuring the stiffness of bacterial cells from growth rates in hydrogels of tunable elasticity. *Mol Microbiol* **84,** 874–891 (2012).
29. Garner, E. C., Bernard, R., Wang, W., Zhuang, X. & Rudner, D. Z. Coupled, circumferential motions of the cell wall synthesis machinery and MreB filaments in B. subtilis. *Science* (2011).
30. Hussain, S. *et al.* MreB Filaments Create Rod Shape By Aligning Along Principal Membrane Curvature. *bioRxiv* 1–94 (2017). doi:10.1101/197475
31. Robertson, G. T. *et al.* A Novel Indole Compound That Inhibits Pseudomonas aeruginosa Growth by Targeting MreB Is a Substrate for MexAB-OprM. *Journal of Bacteriology* **189,** 6870–6881 (2007).
32. Kruse, T., Bork-Jensen, J. & Gerdes, K. The morphogenetic MreBCD proteins of Escherichia coli form an essential membrane-bound complex. *Mol Microbiol* **55,** 78–89 (2005).
33. Bendezú, F. O. & de Boer, P. A. J. Conditional lethality, division defects, membrane involution, and endocytosis in mre and mrd shape mutants of Escherichia coli. *Journal of Bacteriology* **190,** 1792–1811 (2008).
34. McDonald, M. J., Gehrig, S. M., Meintjes, P. L., Zhang, X.-X. & Rainey, P. B. Adaptive divergence in experimental populations of Pseudomonas fluorescens. IV. Genetic constraints guide evolutionary trajectories in a parallel adaptive radiation. *Genetics* **183,** 1041–1053 (2009).
35. Julou, T., Desprat, N., Bensimon, D. & Croquette, V. Monitoring microbial population dynamics at low densities. *Rev Sci Instrum* **83,** 074301 (2012).
36. Julou, T. *et al.* Cell-cell contacts confine public goods diffusion inside Pseudomonas aeruginosa clonal microcolonies. *Proc Natl Acad Sci USA* **110,** 12577–12582 (2013).
37. Locke, J. C. W. & Elowitz, M. B. Using movies to analyse gene circuit dynamics in single cells. *Nature Publishing Group* **7,** 383–392 (2009).
38. Winsor, G. L. *et al.* Enhanced annotations and features for comparing thousands of Pseudomonas genomes in the Pseudomonas genome database. *Nucleic Acids Res* **44,** D646–53 (2016).
39. Kumar, S., Stecher, G. & Tamura, K. MEGA7: Molecular Evolutionary Genetics Analysis Version 7.0 for Bigger Datasets. *Mol Biol Evol* **33,** 1870–1874 (2016).
40. Robert, X. & Gouet, P. Deciphering key features in protein structures with the new ENDscript server. *Nucleic Acids Res* **42,** W320–4 (2014).
41. Humphrey, W., Dalke, A. & Schulten, K. VMD: visual molecular dynamics. *J Mol Graph* **14,** 33–8– 27–8 (1996).
42. Lind, P. A., Farr, A. D. & Rainey, P. B. Experimental evolution reveals hidden diversity in evolutionary pathways. *Elife* (2015). doi:10.7554/eLife.07074.001

43. Liu, J., Dazzo, F. B., Glagoleva, O., Yu, B. & Jain, A. K. CMEIAS: A Computer-Aided System for the Image Analysis of Bacterial Morphotypes in Microbial Communities. **41,** 173–194 (2001).
44. Folland, I., Trione, D. & Dazzo, F. Accuracy of Biovolume Formulas for CMEIAS Computer-Assisted Microscopy and Body Size Analysis of Morphologically Diverse Microbial Populations and Communities. *Microb. Ecol.* 1–15 (2014). doi:10.1007/s00248-014-0410-9
45. Jun, S. & Mulder, B. Entropy-driven spatial organization of highly confined polymers: lessons for the bacterial chromosome. *Proc Natl Acad Sci USA* **103,** 12388–12393 (2006).
46. Jun, S. & Wright, A. Entropy as the driver of chromosome segregation. *Nat Rev Micro* (2010). doi:10.1038/nrmicro2391
47. Begg, K. J. & Donachie, W. D. Division planes alternate in spherical cells of Escherichia coli. *Journal of Bacteriology* **180,** 2564–2567 (1998).
48. Zapun, A., Vernet, T. & Pinho, M. G. The different shapes of cocci. *FEMS Microbiology Reviews* **32,** 345–360 (2008).
49. Pinho, M. G., Kjos, M. & Veening, J.-W. How to get (a)round: mechanisms controlling growth and division of coccoid bacteria. *Nature Publishing Group* **11,** 601–614 (2013).
50. Job, V., Carapito, R., Vernet, T., Dessen, A. & Zapun, A. Common alterations in PBP1a from resistant Streptococcus pneumoniae decrease its reactivity toward beta-lactams: structural insights. *J Biol Chem* **283,** 4886–4894 (2008).
51. Murray, T., Popham, D. L. & Setlow, P. Bacillus subtilis cells lacking penicillin-binding protein 1 require increased levels of divalent cations for growth. *Journal of Bacteriology* **180,** 4555–4563 (1998).
52. Kawai, Y., Daniel, R. A. & Errington, J. Regulation of cell wall morphogenesis in Bacillus subtilis by recruitment of PBP1 to the MreB helix. *Mol Microbiol* **71,** 1131–1144 (2009).
53. Banzhaf, M. *et al.* Cooperativity of peptidoglycan synthases active in bacterial cell elongation. *Mol Microbiol* **85,** 179–194 (2012).
54. Claessen, D. *et al.* Control of the cell elongation-division cycle by shuttling of PBP1 protein in Bacillus subtilis. *Mol Microbiol* **68,** 1029–1046 (2008).
55. Skurnik, D., Roux, D. & Cattoir, V. Enhanced in vivo fitness of carbapenem-resistant oprD mutants of Pseudomonas aeruginosa revealed through high-throughput sequencing. in (2013). doi:10.1073/pnas.1221552110/-/DCSupplemental
56. Shih, Y. L., Kawagishi, I. & Rothfield, L. The MreB and Min cytoskeletal-like systems play independent roles in prokaryotic polar differentiation. **58,** 917–928 (2005).
57. Chien, A.-C., Hill, N. S. & Levin, P. A. Cell Size Control in Bacteria. **22,** R340–R349 (2012).
58. Corbin, B. D., Yu, X.-C. & Margolin, W. Exploring intracellular space: function of the Min system in round-shaped Escherichia coli. *EMBO J* **21,** 1998–2008 (2002).
59. Halatek, J. & Frey, E. Highly canalized MinD transfer and MinE sequestration explain the origin of robust MinCDE-protein dynamics. *CellReports* **1,** 741–752 (2012).
60. Desprat, N., Richert, A., Simeon, J. & Asnacios, A. Creep function of a single living cell. *Biophysj* **88,** 2224–2233 (2005).
61. Typas, A., Banzhaf, M., Gross, C. A. & Vollmer, W. From the regulation of

peptidoglycan synthesis to bacterial growth and morphology. *Nature Publishing Group* **10,** 123–136 (2011).
62. Bigot, S., Sivanathan, V., Possoz, C., Barre, F.-X. & Cornet, F. FtsK, a literate chromosome segregation machine. **64,** 1434–1441 (2007).
63. Lleo, M. M., Canepari, P. & Satta, G. Bacterial cell shape regulation: testing of additional predictions unique to the two-competing-sites model for peptidoglycan assembly and isolation of conditional rod-shaped mutants from some wild-type cocci. *Journal of Bacteriology* **172,** 3758–3771 (1990).
64. Bendezú, F. O. & de Boer, P. A. J. Conditional lethality, division defects, membrane involution, and endocytosis in mre and mrd shape mutants of Escherichia coli. *Journal of Bacteriology* **190,** 1792–1811 (2008).
65. Pérez-Núñez, D. *et al.* A new morphogenesis pathway in bacteria: unbalanced activity of cell wall synthesis machineries leads to coccus-to-rod transition and filamentation in ovococci. *Mol Microbiol* **79,** 759–771 (2011).
66. Lleo, M. M., Canepari, P. & Satta, G. Bacterial cell shape regulation: testing of additional predictions unique to the two-competing-sites model for peptidoglycan assembly and isolation of conditional rod-shaped mutants from some wild-type cocci. *Journal of Bacteriology* **172,** 3758–3771 (1990).
67. Monteiro, J. A. O. M. *et al.* Cell shape dynamics during the staphylococcal cell cycle. *Nat Commun* **6,** 1–12 (2015).
68. Young, K. D. Bacterial Shape: Two-Dimensional Questions and Possibilities. **64,** 223–240 (2010).
69. Koch, A. L. Were Gram-positive rods the first bacteria? *Trends Microbiol* **11,** 166–170 (2003).
70. Errington, J. L-form bacteria, cell walls and the origins of life. *Open Biology* **3,** 120143–120143 (2013).
71. Siefert, J. L. & Fox, G. E. Phylogenetic mapping of bacterial morphology. *Microbiology (Reading, Engl.)* **144 (Pt 10),** 2803–2808 (1998).
72. Stackebrandt, E. & Woese, C. R. A phylogenetic dissection of the family micrococcaceae. *Curr. Microbiol.* **2,** 317–322 (1979).
73. Tamames, J., González-Moreno, M., Mingorance, J., Valencia, A. & Vicente, M. Bringing gene order into bacterial shape. *Trends Genet* **17,** 124–126 (2001).
74. Baidouri, El, F., Venditti, C. & Humphries, S. Independent evolution of shape and motility allows evolutionary flexibility in Firmicutes bacteria. *Nat. ecol. evol.* **1,** 0009–6 (2016).